Bright X-Ray Source from a Laser-Driven Microplasma Waveguide

Longqing Yi,[1,2,*] Alexander Pukhov,[1] Phuc Luu-Thanh,[1] and Baifei Shen[2,3]
[1]Institut für Theoretische Physik I, Heinrich-Heine-Universität Düsseldorf, Düsseldorf 40225, Germany
[2]State Key Laboratory of High Field Laser Physics, Shanghai Institute of Optics and Fine Mechanics, Chinese Academy of Sciences, P.O. Box 800-211, Shanghai 201800, China
[3]Collaborative Innovation Center of IFSA (CICIFSA), Shanghai Jiao Tong University, Shanghai 200240, China
(Received 22 November 2015; published 14 March 2016)

Owing to the rapid progress in laser technology, very high-contrast femtosecond laser pulses of relativistic intensities have become available. These pulses allow for interaction with microstructured solid-density plasma without destroying the structure by parasitic prepulses. This opens a new realm of possibilities for laser interaction with micro- and nanoscale photonic materials at relativistic intensities. Here we demonstrate, for the first time, that when coupled with a readily available 1.8 J laser, a microplasma waveguide (MPW) may serve as a novel compact x-ray source. Electrons are extracted from the walls and form a dense helical bunch inside the channel. These electrons are efficiently accelerated and wiggled by the waveguide modes in the MPW, which results in a bright, well-collimated emission of hard x rays in the range of $1 \sim 100$ keV.

DOI: 10.1103/PhysRevLett.116.115001

During the last decade, the research on high-brightness compact x-ray sources has made significant progress while being motivated by many applications in fundamental science, industry, and medicine. Synchrotrons [1,2] and free-electron lasers [3,4] can now produce x-ray beams with unprecedented photon flux and brilliance. These large facilities are excellent x-ray sources being booked by a large community of international users. However, these are unique, expensive, and large-scale devices. In parallel—as an alternative approach—interest in laser-plasma based sources of secondary radiation is growing constantly [5–8]. The recent progress in laser technologies and laser-plasma acceleration has enabled the development of a compact all-optical Compton source of hard photons [9,10] or a laser-plasma synchrotronlike source [11–14]. Laser beams with intensities of 10^{21} W/cm^2 are readily available at several facilities worldwide [15–18]. The interaction of these ultraintense laser pulses with matter accesses unexplored experimental regimes, ushering in advances in x-ray sources.

For laser-plasma x-ray sources, previous studies have mainly been focused on radiation from electrons generated by laser-driven wakefield accelerators (LWFAs) [19] or hot electrons produced in laser-foil interactions [20–24]. However, the total charge of the electron bunches produced in LWFAs is relatively low owing to the underdense plasma required, which limits the photon yield. On the other hand, in the laser-foil interaction, a high laser-to-photon conversion efficiency ($> 1\%$) can be achieved for a PW laser pulse [24], but the typical radiation divergence is several tens of degrees, making it unsuitable for many applications. Recently, the focus has shifted towards using high contrast laser coupling with structured targets with the aim of increasing laser absorption and the subsequent energy conversion in the secondary radiation [25–27]. With recent advances in laser pulse cleaning techniques, laser peak-to-pedestal contrast ratios higher than 10^{10} have been achieved using the cross-polarized wave generation (XPW) technique [28], which allows for interaction with fine plasma structures such as nanoparticles [29], snowfakes [30], and microplasma waveguides (MPWs) [31]. It has been shown that spatially periodic electron beams with attosecond duration and an over-critical density can be acquired from an intense laser pulse interacting with a MPW [31–33]. These electrons are extracted from the boundary by an intense laser pulse, and accelerated forward via the longitudinal component of the electric field that arises from transverse magnetic (TM) modes [34,35]. Simultaneously, the intrinsic asymmetric transverse fields of the waveguide modes provide efficient wiggling as the superluminal phase overtakes the electrons. Hence, these ultrashort dense energetic electron bunches have the potential to be an excellent source for x-ray emission.

The sketch of our simulation setup is shown in Fig. 1(a). A circularly polarized laser enters the MPW from the left side, the electrons from the skin layer of the channel boundary are extracted into the channel, forming a helical bunch. Electrons with proper phase can be accelerated with a peak acceleration gradient of 4 TV/m as shown in Figs. 1(b) and 1(c). The map of longitudinal fields in the MPW [Figs. 1(b)–1(d)] shows an interference between different optical modes excited in the MPW, which overtake the accelerating electron bunches and wiggle them efficiently. As a result, bright synchrotron radiation is generated in forward direction [Fig. 1(e)]. The waveguide modes slowly separate from each other owing to the different group velocities, some pure high order mode patterns are observed in the rear of the simulation box behind the main laser pulse as shown in Fig. 1(d). Although a similar geometrical setup has been proposed by Bulanov *et al.* [36,37], the underlying physical processes are completely

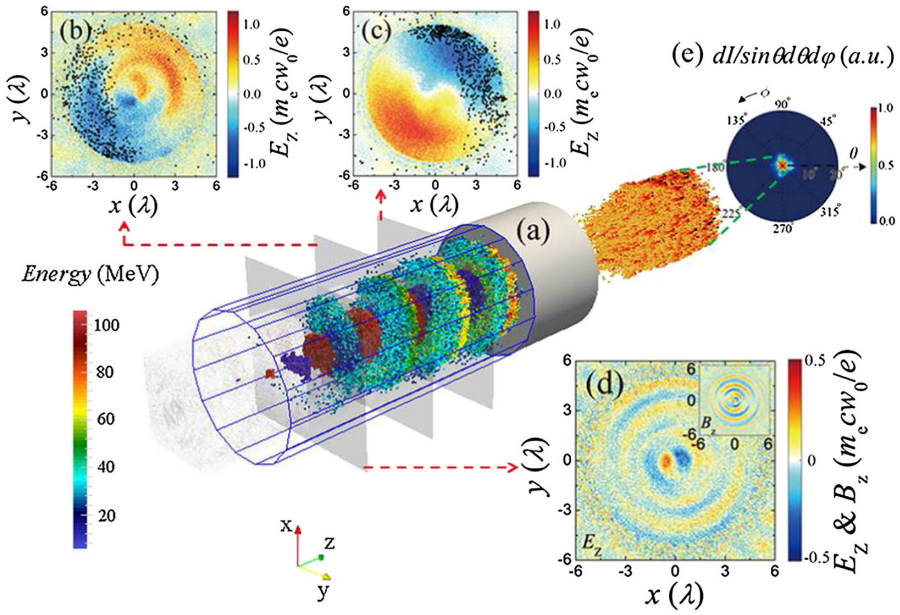

FIG. 1. (a) Sketch of x-ray production by laser interaction with a MPW. When a circularly polarized laser (blue-red sequence in the middle) propagates inside a MPW (white cylinder and blue wireframe), it extracts electrons out of the walls. These electrons form a helical bunch, which oscillates in the laser field and emits x-ray photons (orange block). The longitudinal electric fields of optical modes excited in the MPW are shown at three cross sections: middle slice (b), right slice (c), and left slice (d) at $t = 50T_0$. The colorbar in (a) presents the electron energy at this time. The electron positions at cross sections (b) and (c) are shown by black dots. On the slice (d), we have shown the longitudinal electric field and magnetic field (inset) observed behind the main pulse, where some high-order optical mode patterns can be seen. (e) Typical radiation pattern and divergence. Here θ is the angle between the emission and laser propagation direction. The laser pulse has the wavelength $\lambda_0 = 800$ nm, the pulse energy is 1.8J and the duration is 15 fs. The MPW radius is 4 μm.

different. In the present work, the x-ray emission results from the electron oscillation in superluminal modes, while in Refs. [36,37], the underlying mechanism is the multiple reflection of the laser pulse by relativistic oscillation mirrors (ROMs) [38,39]. Moreover, since the radiation frequency is limited by the density of the channel boundary in the proposed mechanism by Bulanov *et al.*, it is unlikely to produce hard x-ray photons beyond 1 keV as discussed in the remainder of this work.

Keeping in mind the possible applications [40–44] of hard x-ray photons, we focus on the angular distribution of radiation and its spectrum, along with the x-ray generation efficiency. We carried out 3D particle-in-cell (PIC) simulations with the code VLPL [45] to explore the electron dynamics and the synchrotron radiation in the MPW, where a moderately high-intensity Gaussian laser beam with temporal FWHM duration 15 fs, focus spot $3.5\lambda_0$ ($\lambda_0 = 0.8$ μm is the laser wavelength) is employed to drive the MPW x-ray source. The normalized amplitude of the laser is $a_0 = eE_0/m_e c\omega_0 = 15$ (intensity $\sim 10^{20}$ W/cm^2), where E_0 is the amplitude of the laser, m_e is the mass of an electron, e is the unit charge, and ω_0 is the laser frequency. The dimensions of the simulation box are $x \times y \times z = 12\lambda_0 \times 12\lambda_0 \times 20\lambda_0$, and are sampled by $300 \times 300 \times 1000$ cells with 3 particles in each cell. The time step is $dt = 0.016T_0$, where $T_0 = 2.67$ fs is the laser cycle. The MPW has a density of $n_0 = 10n_c$ ($n_c = m_e\omega_0^2/4\pi e^2$ is the critical density), an inner radius of $R_0 = 5\lambda_0$, and longitudinal length of 400 μm. It should be noted although the density of the MPW is limited by computational efficiency, in real experiments, the laser can hardly penetrate into the area with $n > 10n_c$ due to finite density gradients. In addition, the short-wavelength electromagnetic emission is calculated following the approach of classical synchrotron radiation as elucidated in Ref. [8], which has been implemented in PIC codes [46], and demonstrated in several recent experiments [47,48].

Figure 2(a) presents the dependence of radiation intensity on emission angle and photon energy. By integrating over the photon energy, one obtains the dependence of the radiation intensity on the emission angle, as presented by the blue curve in Fig. 2(b). Obviously, the x rays are dominantly in the forward direction, most of the x-ray photons are concentrated in the range of 0–20 mrad, and the radiation intensity decreases rapidly as the observation angle increases beyond 20 mrad. The root mean square (RMS) opening angle is $\theta_{\mathrm{RMS}} = 17$ mrad. Similarly, the red curve in Fig. 2(c) is obtained by integrating the angle dependence in Fig. 2(a), which shows the photon energy spectrum. One can see a broad frequency band covering the total range from soft x rays to hard x rays, with a center frequency around 20 keV.

Figure 2(d) presents the photon yield and radiation energy plotted against the propagation distance; a linear growth is observed up to $150\lambda_0$, which then turns to saturation slowly. The total photon yield is 3×10^{10} /shot. Taking a divergence of 17×17 mrad^2, spot size 16π μm^2, and x-ray pulse duration $\sim$15 fs (equal to the duration of laser pulse), the peak brilliance is 1.4×10^{23} photons/s/mm^2/mrad^2/0.1% bandwidth, comparable to or even greater than state-of-the-art third-generation synchrotron sources. Consider one of the most brilliant x-ray sources, PETRAIII [1] for example. In

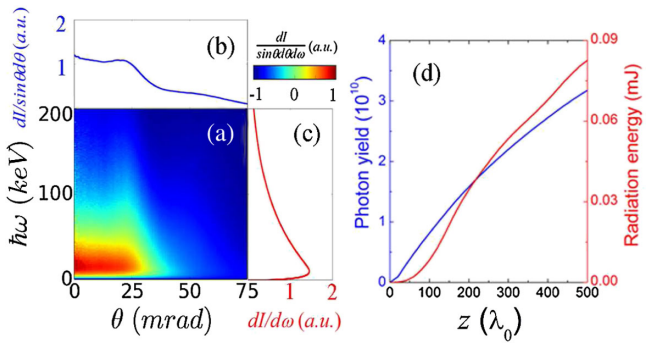

FIG. 2. (a) Angular dependence of the emitted photon energy, and dependence of radiation intensity on (b) angle and (c) photon energy. (d) Total photon yield and radiation energy. Here, θ is the same as in Fig. 1(e).

the energy range of 50–150 keV, the photon flux generated is 10^{13} photons/s/0.1% bandwidth. With an extremely low horizontal emittance (~1 nm rad), the brilliance attained is 10^{20} photons/s/mm^2/mrad^2/0.1% bandwidth, which is 3 orders of magnitudes lower than of the proposed MPW x-ray source. The total radiated energy is 0.09 mJ, while the incident laser energy is about 1.8 J in the simulation, which results in a reasonable laser-to-photon conversation efficiency of 5×10^{-5}.

In order to obtain a deeper insight into the radiation mechanism, we now analyze the electron dynamics in MPWs. Owing to the axially symmetric structure, we consider the cylindrical coordinate system (z, r, ϕ), choosing the z axis as the axis of symmetry of the cylindrical MPW; the laser propagates towards the $+z$ direction. The electric and magnetic fields in a MPW can be expressed in terms of two Hertz potentials Π^e and Π^h [49]:

$$E_z = \frac{\partial^2 \Pi^e}{\partial z^2} + k^2 \Pi^e, \quad H_z = \frac{\partial^2 \Pi^h}{\partial z^2} + k^2 \Pi^h, \tag{1}$$

$$E_r = \frac{\partial^2 \Pi^e}{\partial z \partial r} - i\omega\mu_0 \frac{1}{r}\frac{\partial \Pi^h}{\partial \phi}, \quad H_r = \frac{\partial^2 \Pi^h}{\partial z \partial r} + i\omega\epsilon_0 \frac{1}{r}\frac{\partial \Pi^e}{\partial \phi}, \tag{2}$$

$$E_\phi = \frac{1}{r}\frac{\partial^2 \Pi^e}{\partial z \partial \phi} + i\omega\mu_0 \frac{\partial \Pi^h}{\partial r}, \quad H_\phi = \frac{1}{r}\frac{\partial^2 \Pi^h}{\partial z \partial \phi} - i\omega\epsilon_0 \frac{\partial \Pi^e}{\partial r}, \tag{3}$$

where

$$\Pi^e(z, r, \phi) = \sum_{n,m} a_n^e J_n(T_m r) \sin(n\phi) e^{-ik_z z} + \text{c.c.}, \tag{4}$$

$$\Pi^h(z, r, \phi) = \sum_{n,m} a_n^h J_n(T_m r) \cos(n\phi) e^{-ik_z z} + \text{c.c.} \tag{5}$$

Here, ϵ_0 and μ_0 are the permittivity and permeability of vacuum, a_n^e and a_n^h are coefficients determined by the incident laser amplitude, k_z is the longitudinal wave number, $T_m = \sqrt{k^2 - k_z^2} = x_m/R_0$ is the transverse wave number, and x_m is the mth root of the eigenvalue equation [49]

$$A(n)[B(n) - 2C(n)] + \frac{\omega_p^2}{\omega^2} C(n)K(n) = 0, \tag{6}$$

where

$$A(n) = J(n) + K(n), \tag{7}$$

$$B(n) = A(n) + \frac{\omega_p^2}{\omega^2}[(n/y^2) - K(n)] \tag{8}$$

$$C(n) = n/x^2 + n/y^2, \tag{9}$$

$$J(n) = \frac{J_{n+1}(x)}{xJ_n(x)}, \qquad K(n) = \frac{K_{n+1}(y)}{yK_n(y)}. \tag{10}$$

Here $y = \sqrt{(4\pi R_0^2/\lambda_p^2) - x^2}$, $J_n(x)$ is the Bessel function of the first kind, $K_n(y)$ is the modified Bessel function of the second kind. Since the dominant modes in the MPW are TM_{11} and TE_{11}, in the following we only take these two modes into consideration for simplicity. A brief discussion about the multimode effect will be given after the underlying physics features are addressed. In this case, the amplitude of Hertz potential in Eqs. (4) and (5) can be obtained by $a_1^e = \sqrt{\mu_0/\epsilon_0} a_1^h \approx \sqrt{2} a_0 m_e c\omega_0/ekT_1$.

Since the electron energy plays a key role in the radiation, the acceleration procedure should be discussed first. The energy gain of electrons within the right phase [see Figs. 1(b) and 1(c)] can be calculated as

$$\varepsilon_{\max} \approx e\bar{E}_z L_d \approx \frac{2\pi^2 R_0 a_0}{x_1 \lambda_0} m_e c^2, \tag{11}$$

where $\bar{E}_z \approx TE_0/2k$ is the average longitudinal electric field due to the TM_1 mode, $L_d = 4\pi^2 R_0^2/x_1^2\lambda_0$ is the dephasing distance. By numerically solving Eq. (6), one obtains $x_1 = 2.5$. So the phase velocity and dephasing distance for the TM_1 mode is $v_p \approx 1.0032c$ and $L_d \approx 150\lambda_0$, respectively. The maximum energy attained is $\varepsilon_{\max} \approx 300$ MeV, which agrees with our simulation as shown in Fig. 3. Since the electron bunches ejected into the MPW are overdense [32], the total charge generated is as high as 2.4 nC, which could extract significant energy from the laser pulse in the 400-μm interaction and result in a yield of abundant x-ray photons.

Because the critical frequency of synchrotron radiation is proportional to $\gamma^2 F_\perp$, the energy attained allows the electrons to radiate at high frequency in the x-ray domain. Meanwhile, in order to study the radiation features, one should also take into account the transverse fields in the MPW,

$$F_\perp = \sqrt{F_r^2 + F_\phi^2} \approx \frac{\sqrt{2} m_e c\omega_0 a_0 x_1^2 \lambda_0^2}{8\pi^2 R_0^2} J_0(T_1 r) i e^{-ik_z z} + \text{c.c.}, \tag{12}$$

where we have assumed that the electron velocity is close to the speed of light ($\beta \sim 1$) and that the electromagnetic wave propagates mainly along the z axis, i.e., $T_1/k \ll 1$.

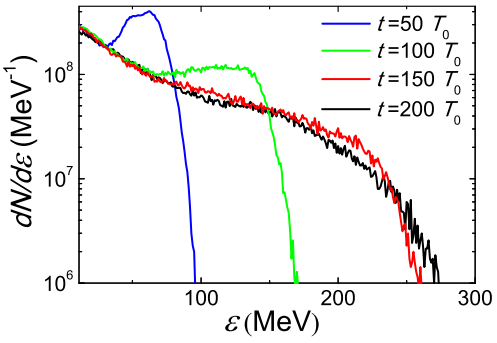

FIG. 3. The electron energy spectrums at different times.

Equations (12) indicate that the optical modes excited in a MPW exert a net transverse force on the ultrarelativistic copropagating electrons. The asymmetry in the transverse electric and magnetic fields arises from the transverse component of the wave number T_1, which induces partial electric (or magnetic) field coupling in the longitudinal direction via reflection by the channel wall. Since the radiation power scales with the square of the transverse force ($P \propto \gamma^2 F_\perp^2$), this asymmetric structure of the waveguide modes greatly enhances photon emission. Figure 4(a) presents the dependance of radiation power on the laser amplitude a_0, which shows a rapid growth as a_0 increases.

When an electron oscillates in an optical mode described by Eqs. (12), the critical frequency is determined by the Lorentz factor of the electron and amplitude of the oscillating transverse field, i.e.,

$$\omega_c = \frac{3\sqrt{2}\bar{\gamma}^2 x_1^2 \lambda_0^2 a_0}{16\pi^2 R_0^2}\omega_0 \approx \frac{3\sqrt{2}\pi^2 a_0^3}{16}\omega_0. \tag{13}$$

Equation (13) allows us to estimate the emitted photon energy. By taking $a_0 = 15$, $R_0 = 5\lambda_0$, the average Lorentz factor $\bar{\gamma} \approx \gamma_{\max}/2 \approx 300$, we obtain the critical frequency $\hbar\omega_c \approx 15$ keV, which agrees well with our PIC simulations as seen in Figs. 2(a) and 2(c). The average photon energy (total radiation energy divided by photon yield) is plotted as a function of laser amplitude a_0 for a fixed channel radius $R_0 = 5\lambda_0$ in Fig. 4(a). It is shown that the numerical observation can be fitted by cube scaling, as suggested by Eq. (13).

The divergence of the radiation is determined by the maximum angle between the electron velocity and propagation axis. The highly collimated photon beam can be attributed to the relatively small transverse wiggling force in a MPW [$\sim 0.01 eE_0$ as suggested by Eq. (12)] and sufficient acceleration can be attained. As the electrostatic field in the MPW is eliminated by the magnetic field due to the surface current [50], one can estimate the maximum transverse displacement for a near axis electron [$J_0(T_1 r) \approx 1$] by double integrating Eq. (12),

$$r_{\max} \approx \frac{4\sqrt{2}\pi R_0^2 a_0}{x_1^2 \lambda_0 \bar{\gamma}}. \tag{14}$$

Therefore, the maximum opening angle of the radiation cone can be calculated as

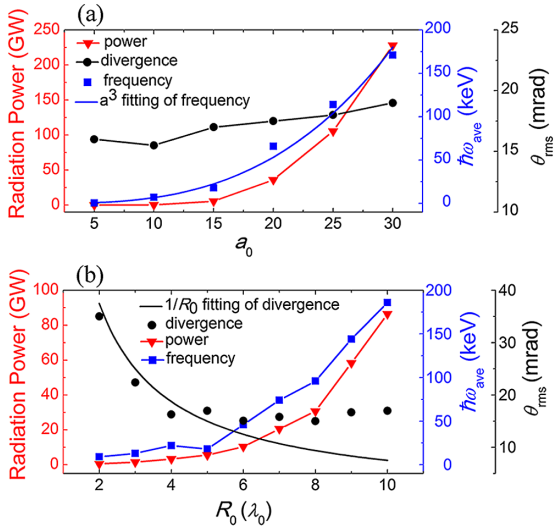

FIG. 4. Dependence of synchrotron radiation power (red triangles), frequency (blue squares) and RMS opening angle (black circles) on (a) laser amplitude and (b) channel radius. The blue curve in (a) shows the a_0^3 fitting of average photon energy, and the black curve in (b) presents the $1/R_0$ fitting of divergence.

$$\Psi = \frac{2\pi r_{\max}}{\lambda_u} \approx \frac{\sqrt{2}a_0}{\bar{\gamma}} \approx \frac{\sqrt{2}x_1\lambda_0}{\pi^2 R_0}, \tag{15}$$

where $\lambda_u \approx 8\pi^2 R_0^2/x_1^2\lambda_0$ is the wiggler spatial period. Equation (15) provides an estimate of the maximum radiation divergence of 70 mrad, which agrees with our numerical observations in Fig. 2(b). Furthermore, Eq. (15) indicates for a fixed MPW, the radiation divergence does not depend on a_0, which is confirmed by our PIC simulation as shown in Fig. 4(a). Moreover, from Eq. (15), one can also obtain the wiggler strength by [5] $K = \bar{\gamma}\Psi \approx \sqrt{2}a_0$.

Finally, we discuss the multimode effects in the MPW. As a laser pulse propagates in the MPW, many modes are excited simultaneously, and the electron motion is subjected to the combined fields of these modes. Normally, the energy proportion coupled into different modes is mainly dependant on the MPW radius, which makes it an important degree of freedom to adjust the radiation power and photon energy. In addition, the phase front curvature and nonsymmetric structure can also affect the coupling conditions, a detailed discussion can be found in Refs. [51–54].

Typically, higher order modes produce a larger transverse wiggling force as more energy is coupled into longitudinal fields in these cases. Hence the critical frequency and radiation power are enhanced if other parameters remain the same. However, due to the difficulty in obtaining the exact amplitudes and energy loss rate for each optical mode in the MPW, one has to rely on PIC simulations to study the effects induced by high-order optical modes. As it can be seen in Fig. 4(b), the average energy of synchrotron photons and radiation power remains almost unchanged when R_0 is small and starts to grow with R_0 when it exceeds $6\lambda_0$ (laser amplitude is fixed at $a_0 = 15$

and the spot size varies proportional to the channel radius). Simultaneously, the divergence of radiation departs from the $1/R_0$ scaling predicted by Eq. (15). This indicates the excitation of higher optical modes so that the transverse force cannot be estimated by considering the TM_{11} and TE_{11} modes alone. Our numerical results show when increasing the MPW radius, the radiation power is enhanced, and the photon energy increases, while the RMS opening angle decreases and saturates at around 15 mrad as presented in Fig. 4(b).

In conclusion, the interaction of electrons with electromagnetic modes in a MPW has been studied through 3D PIC simulations and theoretical analysis. The proposed novel mechanism has the potential to accelerate electrons to several hundreds of MeV and efficiently wiggle them, resulting in the emission of hard photons with high brightness, broad bandwidth, and very low divergence. The underlying physics is discovered, which can be attributed to the fierce acceleration via the longitudinal electric field of TM modes, as well as the asymmetric structure of transverse optical mode components. We also discussed the effects of high-order optical modes, which have the ability to enhance the radiation power and photon energy. These effects become increasingly important as the channel radius increases. The emitted tunable brilliant x rays and γ rays have promising features and might have diverse applications in imaging, medical treatment, isotope production, following chemical processes, and nuclear physics.

We thank Dr. L. L. Ji, Dr. Z. Y. Chen, and Dr. J. Farmer for fruitful discussions and language editing. This work is supported in parts by EUCARD-2, Deutsche Forschungsgemeinschaft SFB TR 18 and National Natural Science Foundation of China (No. 11505262, No. 11125526, and No. 11335013).

*To whom all correspondence should be addressed.
yi@uni-duesseldorf.de

[1] D. Bilderback, P. Elleaume, and E. Weckert, J. Phys. B **38**, S773 (2005).
[2] J. Bahrdt, A. Gaupp, W. Gudat, M. Mast, K. Molter, W. Peatman, M. Scheer, Th. Schroeter, and Ch. Wang, Rev. Sci. Instrum. **63**, 339 (1992).
[3] E. A. Schneidmiller and M. V. Yurkov, Phys. Rev. ST Accel. Beams **16**, 110702 (2013).
[4] M. Altarelli, High Power Laser Sci. Eng. **3**, e18 (2015).
[5] S. Corde, K. Phuoc, G. Lambert, R. Fitour, V. Malka, A. Rousse, A. Beck, and E. Lefebvre, Rev. Mod. Phys. **85**, 1 (2013).
[6] S. Kiselev, A. Pukhov, and I. Kostyukov, Phys. Rev. Lett. **93**, 135004 (2004).
[7] I. Kostyukov, S. Kiselev, and A. Pukhov, Phys. Plasmas **10**, 4818 (2003).
[8] T. P. Yu, A. Pukhov, Z. M. Sheng, F. Liu, and G. Shvets, Phys. Rev. Lett. **110**, 045001 (2013).
[9] N. Powers, I. Ghebregziabher, G. Golovin, C. Liu, S. Chen, S. Banerjee, J. Zhang, and D. Umstadter, Nat. Photonics **8**, 28 (2014).
[10] K. Phuoc, S. Corde, C. Thaury, V. Malka, A. Tafzi, J. Goddet, R. Shah, S. Sebban, and A. Rousse, Nat. Photonics **6**, 308 (2012).
[11] S. Lee, T. Lee, D. Gupta, H. Uhm, and H. Suk, Plasma Phys. Controlled Fusion **57**, 075002 (2015).
[12] M. Chen, J. Luo, F. Li, F. Liu, Z. Sheng, and J. Zhang, Light Sci. Appl. **5**, e16015 (2015).
[13] H. Wang, B. Liu, X. Yan, and M. Zepf, Phys. Plasmas **22**, 033102 (2015).
[14] B. Liu, R. Hu, H. Wang, D. Wu, J. Liu, C. Chen, J. Meyer-ter-Vehn, X. Yan, and X. He, Phys. Plasmas **22**, 080704 (2015).
[15] H. J. Kong, S. Park, S. Cha, H. Ahn, H. Lee, J. Oh, B. J. Lee, S. Choi, and J. S. Kim, High Power Laser Sci. Eng. **3**, e1 (2015).
[16] Extreme Light Infrastructure European Project, https://eli-laser.eu/.
[17] V. Yanovsky, V. Chvykov, G. Kalinchenko, P. Rousseau, T. Planchon, T. Matsuoka, A. Maksimchuk, J. Nees, G. Cheriaux, G. Mourou, and K. Krushelnick, Opt. Express **16**, 2109 (2008).
[18] R. Li, X. Liang, Z. Gan, H. Lu, L. Yu, D. Yin, Y. Leng, X. Lu, C. Wang, and Z. Xu, in Proceedings of 4th Advanced Lasers and Photon Sources (ALPS'15), Yokohama, Yapan, 22-24 April (2015).
[19] T. Tajima and J. M. Dawson, Phys. Rev. Lett. **43**, 267 (1979).
[20] J. D. Kmetec, C. L. Gordon, J. J. Mackin, B. E. Lemoff, G. Brown, and S. Harris, Phys. Rev. Lett. **68**, 1527 (1992).
[21] S. Hatchett *et al.*, Phys. Plasmas **7**, 2076 (2000).
[22] T. Nakamura, J. K. Koga, T. Z. Esirkepov, M. Kando, G. Korn, and S. Bulanov, Phys. Rev. Lett. **108**, 195001 (2012).
[23] C. Courtois, A. Fontaine, O. Landoas, G. Lidove, V. Meot, P. Morel, R. Nuter, E. Lefebvre, A. Boscheron, J. Grenier, M. Aleonard, M. Gerbaux, F. Gobet, F. Hannachi, G. Malka, J. Scheurer, and M. Tarisien, Phys. Plasmas **16**, 013105 (2009).
[24] E. Nerush, I. Kostyukov, L. Ji, and A. Pukhov, Phys. Plasmas **21**, 013109 (2014).
[25] G. Cristoforetti, A. Anzalone, F. Baffigi, G. Bussolino, G. Arrigo, L. Fulgentini, A. Giulietti, P. Koester, L. Labate, S. Tudisco, and L. Gizzi, Plasma Phys. Controlled Fusion **56**, 095001 (2014).
[26] S. Kahaly, S. Yadav, W. M. Wang, S. Sengupta, Z. M. Sheng, A. Das, P. K. Kaw, and G. R. Kumar, Phys. Rev. Lett. **101**, 145001 (2008).
[27] M. Purvis, V. Shlyaptsev, R. Hollinger, C. Bargsten, A. Pukhov, A. Prieto, Y. Wang, B. Luther, L. Yin, S. Wang, and J. Rocca, Nat. Photonics **7**, 796 (2013).
[28] A. Jullien, S. Kourtev, O. Albert, G. Cheriaux, J. Etchepare, N. Minkovski, and S. M. Saltiel, Appl. Phys. B **84**, 409 (2006).
[29] P. Rajeev, P. Ayyub, S. Bagchi, and G. Kumar, Opt. Lett. **29**, 2662 (2004).
[30] A. Zigler, S. Eisenman, M. Botton, E. Nahum, E. Schleifer, A. Baspaly, I. Pomerantz, F. Abicht, J. Branzel, G. Priebe, S. Steinke, A. Andreev, M. Schnuerer, W. Sandner, D. Gordon, P. Sprangle, and K. W. D. Ledingham, Phys. Rev. Lett. **110**, 215004 (2013).

[31] D. Zou, H. Zhuo, T. Yu, H. Wu, X. Yang, F. Shao, Y. Ma, Y. Yin, and Z. Ge, Phys. Plasmas **22**, 023109 (2015).
[32] N. Naumova, I. Sokolov, J. Nees, A. Maksimchuk, V. Yanovsky, and G. Mourou, Phys. Rev. Lett. **93**, 195003 (2004).
[33] Y. T. Li, X. H. Yuan, M. H. Xu, Z. Y. Zheng, Z. M. Sheng, M. Chen, Y. Y. Ma, W. X. Liang, Q. Z. Yu, Y. Zhang, F. Liu, Z. Wang, Z. Wei, W. Zhao, Z. Jin, and J. Zhang, Phys. Rev. Lett. **96**, 165003 (2006).
[34] A. G. York, H. M. Milchberg, J. P. Palastro, and T. M. Antonsen, Phys. Rev. Lett. **100**, 195001 (2008).
[35] R. England *et al.*, Rev. Mod. Phys. **86**, 1337 (2014).
[36] S. Bulanov, F. Kamenents, F. Pegoraro, and A. Pukhov, Phys. Lett. A **195**, 84 (1994).
[37] S. V. Bulanov, T. Z. Esirkepov, N. M. Naumova, and I. V. Sokolov, Phys. Rev. E **67**, 016405 (2003).
[38] S. Bulanov, N. Naumova, and F. Pegoraro, Phys. Plasmas **1**, 745 (1994).
[39] R. Lichters, J. Meyer-ter-Vehn, and A. Pukhov, Phys. Plasmas **3**, 3425 (1996).
[40] S. Kneip *et al.*, Nat. Phys. **6**, 980 (2010).
[41] S. Cipiccia *et al.*, Nat. Phys. **7**, 867 (2011).
[42] C. Boeglin, E. Beaurepaire, V. Halte, V. Flores, C. Stamm, N. Pontius, H. Durr, and J. Bigot, Nature (London) **465**, 458 (2010).
[43] D. Fritz *et al.*, Science **315**, 633 (2007).
[44] R. Neutze, R. Wouts, D. Spoel, E. Weckert, and J. Hajdu, Nature (London) **406**, 752 (2000).
[45] A. Pukhov, J. Plasma Phys. **61**, 425 (1999).
[46] I. Kostyukov, S. Kiselev, and A. Pukhov, Phys. Plasmas **10**, 4818 (2003).
[47] C. Ridgers, C. Brady, R. Duclous, J. Kirk, K. Bennett, T. Arber, A. Robinson, and A. Bell, Phys. Rev. Lett. **108**, 165006 (2012).
[48] M. Schnell, A. Sävert, I. Uschmann, M. Reuter, M. Nicolai, T. Kämpfer, B. LandgrafO. Jäckel, O. Jansen, A. Pukhov, M. C. Kaluza, and C. Spielmann, Nat. Commun. **4**, 2421 (2013).
[49] H. Shen, J. Appl. Phys. **69**, 6827 (1991).
[50] S. Jiang, A. G. Krygier, D. W. Schumacher, K. U. Akli, and R. R. Freeman, Phys. Rev. E **89**, 013106 (2014).
[51] B. Cros, C. Courtois, G. Matthieussent, A. DiBernardo, D. Batani, N. Andreev, and S. Kuznetsov, Phys. Rev. E **65**, 026405 (2002).
[52] M. Veysman, N. E. Andreev, K. Cassou, Y. Ayoul, G. Maynard, and B. Cros, J. Opt. Soc. Am. B **27**, 1400 (2010).
[53] M. Veysman, N. E. Andreev, G. Maynard, and B. Cros, Phys. Rev. E **86**, 066411 (2012).
[54] N. Andreev, S. Kuznetsov, and M. Veysman, Nucl. Instrum. Methods Phys. Res., Sect. A **740C**, 273 (2014).